Beyond the Rayleigh Criterion: Grating Assisted Far-Field Optical Diffraction Tomography

Anne Sentenac, Patrick C. Chaumet, and Kamal Belkebir

Institut Fresnel (UMR 6133), Université Paul Cézanne and Université de Provence, F-13397 Marseille Cedex 20, France

(Received 5 July 2006; published 11 December 2006)

We propose an optical imaging system, in which both illumination and collection are done in far field, that presents a power of resolution better than one-tenth of the wavelength. This is achieved by depositing the sample on a periodically nanostructured substrate illuminated under various angles of incidence. The superresolution is due to the high spatial frequencies of the field illuminating the sample and to the use of an inversion algorithm for reconstructing the map of relative permittivity from the diffracted far field. Thus, we are able to obtain wide-field images with near-field resolution without scanning a probe in the vicinity of the sample.

DOI: 10.1103/PhysRevLett.97.243901 PACS numbers: 42.30.Wb, 42.25.Fx

Developing optical imaging systems with sub-100 nm resolution stirs a considerable interest especially in the nanotechnology and biology domains. The barrier to be broken is the well-known Rayleigh criterion that states that two radiating dipoles are distinguishable on the image of their far-field intensity if their interdistance is greater than 0.6λ where λ is the wavelength of radiation. This intrinsic limitation, caused by light diffraction, applies, in particular, to classic optical microscopes [1]. Shortening the wavelength of radiation with immersion techniques [2], the use of hemispherical prisms [3,4] or the excitation of surface plasmons [5,6] has permitted the increase of the power of resolution of these systems. Yet, due to the narrow range of available transparent material in optics, the power of resolution remains close to 150 nm for a free-space wavelength of 500 nm. A similar result has been obtained with the so-called silver superlens imaging technique [7]. The breakthroughs in high resolution optical imaging have been obtained in near-field optical microscopy by scanning a probe in subwavelength proximity to the sample [8], and more recently, in far-field fluorescence microscopy by taking advantage of nonlinear effects [9] and the use of structured illumination [10,11]. Yet, these spectacular ameliorations of the resolution are achieved at the expense of a certain readiness or versatility of utilization, probe scanning, or need for fluorescent objects.

In this Letter, we propose an optical imaging system dedicated to nonfluorescent objects that presents a nanometer-scale resolution without resorting to probe scanning or nonlinear phenomena. Our approach relies on diffraction tomography principles, a relatively new imaging technique in optics which is closely related to that developed in the microwave or acoustic domains. In an optical diffraction tomography (ODT) experiment, the sample is illuminated by a laser beam along different successive directions of incidence and the amplitude and phase of the far field is detected for many angles of observations. Note that the problem of measuring the phase of the diffracted field in this configuration has been solved experimentally with an astute interferometric setup by [12]. The image, or map of relative permittivity of the sample, is then numerically synthesized from the diffracted far-field data. The inversion algorithm uses the fact that, under single scattering approximation, when a sample is illuminated by a monochromatic plane wave with wave vector $\mathbf{k}^{\mathrm{inc}}$, its diffracted far field in the direction given by the wave vector $\mathbf{k}^{\mathrm{diff}}$ yields the spatial Fourier transform of the sample permittivity, $\hat{\varepsilon}(\mathbf{k}^{\mathrm{inc}} - \mathbf{k}^{\mathrm{diff}})$. Hence, in an ideal optical diffraction tomography system with all possible angles of incidence and detection, the resolution is about 0.3λ, already half that obtained with a classical microscope [12]. From these considerations, it is easily seen that the power of resolution of ODT is all the better than the spatial frequency of the field incident on the sample is high. Hence, it has been proposed to deposit the objects on a prism and to illuminate them under total internal reflection [13]. In total internal reflection tomography (TIRT), the highest spatial frequency of the incident field in the plane of the substrate is n/λ, where n is the index of refraction of the prism. Recent numerical simulations have shown that, in this case, a resolution of $0.6\lambda/(n+1)$ can be expected [14]. Thus, to reach a power of resolution comparable to that of near-field optical microscopes or saturated fluorescent microscopes, it is necessary to overcome the bounds imposed by the available refraction indices in the optical domain to generate high-spatial-frequency incident fields. For example, this can be obtained with a combination of ODT and near-field microscopy by scanning a diffractive element in the near zone of the sample [15]. Yet, this technique is still hampered by the need of moving an object close to the sample. To the contrary, our approach does not borrow any features to near-field microscopy inasmuch as the near-field resolution is reached with a classical far-field ODT setup [12,14] by depositing the sample on a periodically nanostructured substrate, see Fig. 1.

We consider a biperiodic grating that is illuminated from below by a plane wave with wave vector $\mathbf{k}^{\mathrm{inc}} = (\mathbf{k}_{\parallel}^{\mathrm{inc}}, k_z^{\mathrm{inc}})$ where, the subscript $\parallel$ indicates the projection onto the plane of the substrate while the subscript z indicates the projection onto the normal of the substrate plane. The field above the grating, for $z > 0$, can be written as a Rayleigh series,

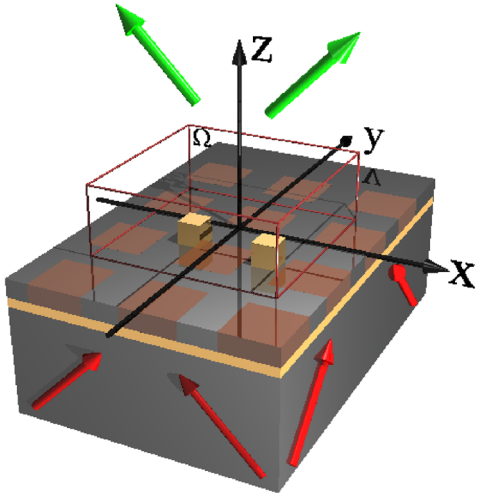

FIG. 1 (color online). Geometry of the imaging system. the objects are deposited on a nanostructured substrate and successively illuminated from below by eight plane waves. The incident angle with respect to Oz is always 80° while the incident angle with respect to Ox varies with a step of 45°. The far field is detected above the substrate along 64 directions equally spaced within a cone of half-angle 80°. The sample is made of two cubes with side $\lambda/20$ and centers interdistance $\lambda/10$.

$$\mathbf{E}_{\text{ref}}(\mathbf{k}_{\parallel}^{\text{inc}}, \mathbf{r}_{\parallel}, z) = \sum_{\mathbf{K}\in W} \mathbf{E}_{\mathbf{K}}(\mathbf{k}_{\parallel}^{\text{inc}}) e^{i[(\mathbf{K}+\mathbf{k}_{\parallel}^{\text{inc}})\cdot\mathbf{r}_{\parallel}+ik_z z]}, \quad (1)$$

where W denotes the reciprocal space of the periodic structure, $k_z = [k_0^2 - |\mathbf{K} + \mathbf{k}_{\parallel}^{\text{inc}}|^2]^{1/2}$ with imaginary part of k_z positive, and the dependence in $\exp(-i\omega t)$ with $k_0 = 2\pi/\lambda = \omega/c$ is omitted. From Eq. (1) it is easily seen that provided that $\mathbf{E}_{\mathbf{K}}$ does not decay too quickly with increasing $\mathbf{K}$, the field incident on the sample will present high spatial frequencies. Now, to use the simple relationship between the diffracted far field and the Fourier coefficient of the sample permittivity, it is preferable that one order, denoted by $\mathbf{E}_{\mathbf{K}_c}$, be predominant in Eq. (1). One solution consists in using the periodic nanostructuration as a grating coupler for high-frequency surface modes such as those supported by metallic films. Indeed, it is well known that metallic layers support surface plasmons whose wave vectors $\mathbf{k}_p$ are all the larger than their thickness is small [16]. These plasmons can be coupled, via the grating, to a free-space incident plane wave if there exists one vector of the reciprocal space $\mathbf{K}_c$ such that

$$\mathbf{k}_p \approx \mathbf{k}_{\parallel}^{\text{inc}} + \mathbf{K}_c. \quad (2)$$

Unfortunately, contrary to long-range plasmons, plasmons whose wave vector modulus is much larger than the free-space wave number k_0 present high losses. Hence, they are difficult to excite even with an optimized periodic perturbation. In all the structures we have studied, the field amplitude $\mathbf{E}_{\mathbf{K}_c}$, which bears the signature of the plasmon excitation, turned out to be comparable to the specular transmitted amplitude $\mathbf{E}_{\mathbf{0}}$. Hence, the relationship between the far-field data and the permittivity is not as simple as in the usual ODT, since the object is illuminated simultaneously by several plane waves. Moreover, due to the interferences, the field intensity at the surface of the grating is strongly inhomogeneous. To avoid the formation of blind and bright spots, it is necessary to check that the average of the illumination over all the incidences is roughly homogeneous within one period of the grating. This can be obtained with a weak periodic modulation. Bearing these requirements in mind, we designed a substrate consisting in a 7 nm silver film, deposited on a glass prism, and surmounted by a 7 nm layer of SiO_2. This last layer is etched periodically with square holes that are filled with Ta_2O_5. Hence, the nanostructure is a phase grating with relatively small contrast $n_{SiO_2} = 1.5$, $n_{Ta_2O_5} = 2.1$ and presents flat interfaces. The square period d of the bidimensional grating is 100 nm while the side of the holes is 67 nm and the free-space wavelength of illumination $\lambda = 500$ nm. The short-range plasmon that can be excited with this structure, taking $n_{\text{silver}} = 0.12 + 2.91i$ has a wave number close to $6k_0$, much larger than that obtained with usual plasmon-assisted sensors. The incident wave vector is taken in the Oxz plane with an angle of incidence of 80° that roughly satisfies Eq. (2) with $\mathbf{K}_c = \frac{2\pi}{d}\hat{\mathbf{x}}$. To excite the plasmon, the incident polarization is also in the Oxz plane. We have used eight different illuminations by rotating the incident plane of 45° about the z axis. In Fig. 2 we plot the modulus of the field just above the grating for various angles of incidence and we verify that, eventually, the grating surface is illuminated rather homogeneously.

We have simulated a grating-assisted diffraction tomography experiment with a rigorous numerical method based on the coupled dipole technique. This tool permits one to calculate the field diffracted by an aperiodic object depos-

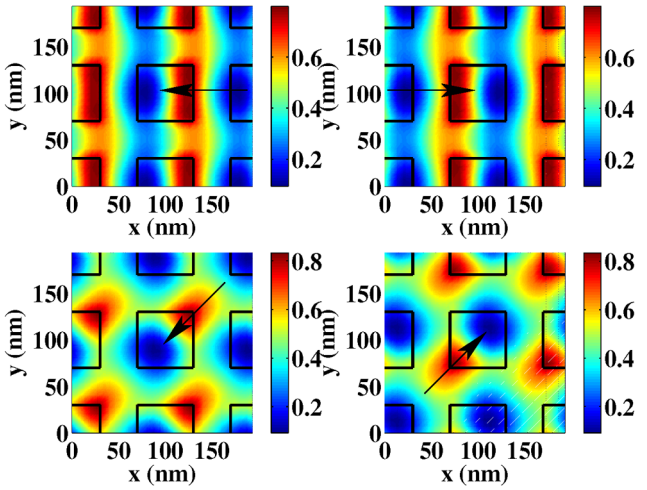

FIG. 2 (color online). Modulus of the field above the grating at the altitude $z = 10$ nm for various incident angles. The projection of the incident wave vector onto the Oxy plane is represented by an arrow. One observes that the bright and dark spots vary with the incident direction.

ited on a periodically structured substrate [17]. The diffracted field is evaluated (both in amplitude and phase) for 64 directions of observation homogeneously spaced in a cone of half-angle 80° above the substrate for each eight illuminations. The unavoidable experimental noise is taken into account by corrupting the simulated data with an additive complex uniform noise with an amplitude equal to 10% of the diffracted field modulus. Then, the permittivity distribution ε of the sample is determined by minimizing the cost functional [14],

$$\mathcal{F}(\varepsilon) = \sum_{\mathbf{k}^{\mathrm{inc}},\mathbf{k}^{\mathrm{diff}}} \| \mathbf{F}(\mathbf{k}^{\mathrm{inc}},\mathbf{k}^{\mathrm{diff}}) - \mathbf{E}(\mathbf{k}^{\mathrm{inc}},\mathbf{k}^{\mathrm{diff}},\varepsilon) \|^2, \quad (3)$$

where $\mathbf{F}$ is the "experimental" data and $\mathbf{E}$ is the simulated field radiated by the best available estimated permittivity ε. More precisely, we assume that the sample is included in a bounded domain Ω above the grating (see Fig. 1) and ε is deduced iteratively at the nodes of a regular meshing of Ω with a conjugate gradient algorithm. To speed up the inversion procedure, $\mathbf{E}$ is evaluated under the extended Born approximation [14] or by replacing the nanostructured top layer by a homogeneous film.

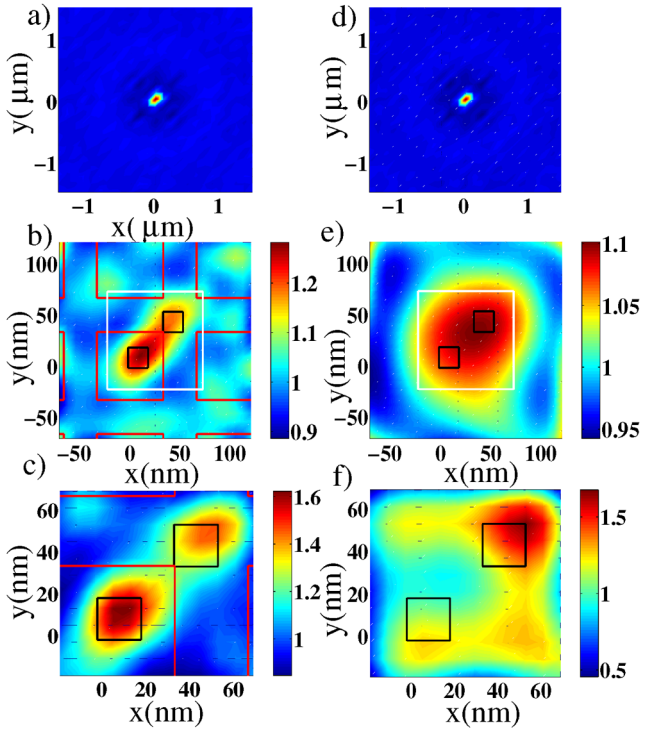

FIG. 3 (color online). Map in the (x, y) plane at altitude $z = 12$ nm of the real part of the permittivity for various investigation domains Ω obtained with the inversion procedure from the diffracted far-field data. (a)–(c) The objects are deposited on the nanostructured substrate. (e)–(g) The objects are deposited on the same substrate with the nanostructured top layer replaced by an homogeneous film with same thickness and permittivity 2.25. When present, the positions of the high index motif of the grating are indicated with squares. The investigation domain volume is $6\lambda \times 6\lambda \times \lambda/2$ in (a) and (e), $\lambda/2 \times \lambda/2 \times \lambda/5$ in (b) and (f), and $\lambda/5 \times \lambda/5 \times \lambda/10$ in (c) and (g).

In a first example, we study the image of two dipolelike objects, namely, two cubes of glass with side $\lambda/20$. The interdistance between the cube centers is taken equal to $\lambda/10$, thus much smaller than the Rayleigh criterion. To assess the role of the grating in the enhanced resolution, we compare the reconstructed permittivity obtained when the objects are deposited on the nanostructured substrate to that obtained when the nanostructured top layer is replaced by a homogeneous film with the same thickness and permittivity 2.25. The inversion procedures in these two configurations differ solely by the use of different Green tensors for calculating the illumination and the far field [14,17]. In Fig. 3, we present the map of permittivity obtained with the inversion algorithms for different domains Ω of investigation. In Figs. 3(a) and 3(d) the domain Ω covers $6\lambda \times 6\lambda \times \lambda/2$ with a mesh side about $\lambda/2$. The reconstructed relative permittivity points out the ability of our technique to localize the objects whatever the substrate. Then, we diminish the size of the investigation domain Ω to $\lambda/2 \times \lambda/2 \times \lambda/5$ and we reconstruct the permittivity over a meshing of side $\lambda/60$, see Figs. 3(b) and 3(e). We observe already that the reconstructed permittivity is more accurate when the objects are deposited on the grating than when they are deposited on the homogeneous metallic multilayer. To ameliorate further the resolution, we focus in the zone of interest, indicated by the white lines in Figs. 3(b) and 3(e), while keeping the same mesh size. Indeed, decreasing the data-to-unknown ratio generally allows one to improve the reconstruction. With the nanostructured substrate, Fig. 3(c), the two cubes are now clearly distinguishable while, with the layered substrate, Fig. 3(f) the image is a nonsense that depends

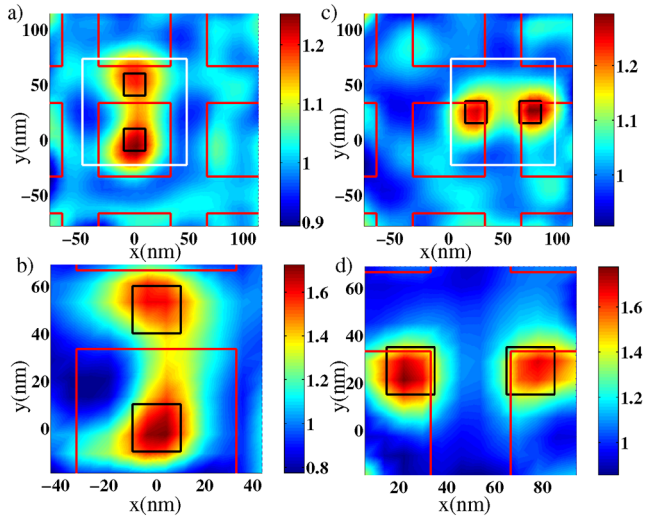

FIG. 4 (color online). (a),(c) Map in the (x, y) plane at altitude $z = 12$ nm of the real part of the permittivity for different positions of the objects with respect to the grating. (b),(d) idem (a),(c) but with a smaller investigation domain indicated with white lines in (a),(c). Ten different positions and orientations of the objects have been studied. Sole the worst and best reconstructions are presented.

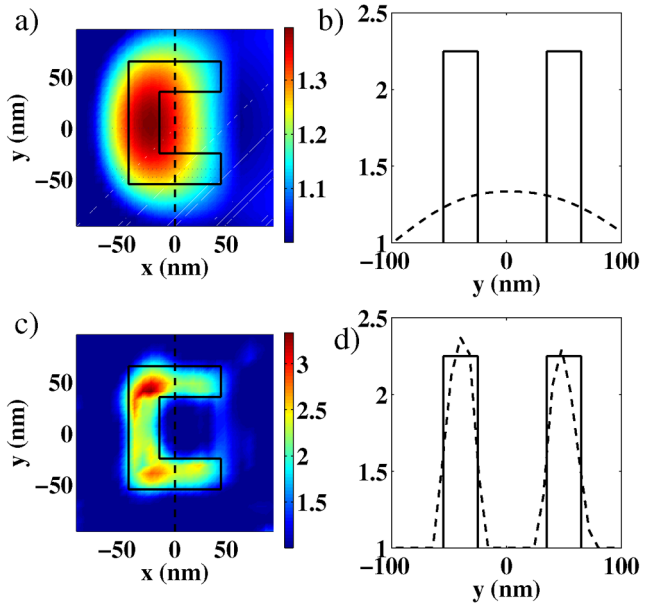

FIG. 5 (color online). Plain lines in (a),(b) [(c),(d)] indicate the real shape (permittivity profile) of the object. (a),(b) The C-shaped object is deposited on the homogeneous layered substrate. Map in the Oxy plane at altitude $z = 4$ nm of the real part of the reconstructed permittivity for a C-shaped object deposited on an homogeneous layered substrate, (b) plot of the estimated permittivity along the dash line in (a). (c) and (d) same as (a) and (b) but the nanostructured layer is replaced by an homogeneous film as in Fig. 3.

strongly on the noise. This focusing technique can be used to obtain wide-field images of more complex samples. First, the objects scattered on the substrate are localized with a coarse meshing, then, several disjoined investigation domains with smaller meshes are generated about their location to improve the resolution.

Since the nanostructured substrate is not invariant by translation, it is necessary to check the influence of the relative position of the objects with respect to the grating on the resolution. In Fig. 4, we present the worst and the best images that we have obtained for ten different positions of the cubes. It is always possible to distinguish precisely the two cubes. The width at midheight of the peaks is about $\lambda/12$. This resolution is in agreement with the criterion obtained in the TIRT configuration $0.6\lambda/(n_p + 1)$, where n_p is the effective index of the plasmon, $k_p = n_p k_0 \approx 6k_0$.

In a second example, Fig. 5, we present the reconstructed permittivity of a C-shaped object with a relative permittivity of 2.25. In Figs. 5(a) and 5(b) the object is deposited on the homogeneous multilayer. One observes that the shape of the object is not retrieved and that the value of the permittivity is badly estimated. On the contrary, when the object is deposited on the nanostructured substrate, Figs. 5(c) and 5(d), the topography of the object is well described and the permittivity is accurately estimated. The role of the grating is again clearly demonstrated.

We have shown the interest and the feasibility of a grating-assisted optical diffraction tomography experiment for obtaining wide-field, highly resolved images. In our imaging system, the grating is used as a delocalized probe in order to generate evanescent waves with high spatial frequencies at each point of the substrate. The reconstruction algorithm is simple and fast since linear inversion using the extended Born approximation is sufficient in most cases. The image resolution is not limited by the wavelength of illumination but depends on the ability of the grating to generate electromagnetic field with high spatial frequencies. Hence, it is linked essentially to the period of the grating. The proposed nanostructured substrate can be realized with present nanolithography techniques but gratings with period smaller than 100 nm yielding better resolution could be envisaged in the future. Last, our system can easily be adapted to fluorescent imaging with structured illumination without saturation. [11,18].

This work was supported by a grant of the Ministère de la Recherche, No. ACI 02 2 0225, and the Conseil Général des Bouches du Rhône and the Conseil Régional PACA. The authors would like to thank Frédéric Forestier for the computer science support.

[1] N. Streibl, J. Opt. Soc. Am. A **2**, 121 (1985).
[2] D. Courjon, K. Sarayeddine, and M. Spajer, Opt. Commun. **71**, 23 (1989).
[3] S. B. Ippolito, B. B. Goldberg, and M. S. Unlu, Appl. Phys. Lett. **78**, 4071 (2001).
[4] G. E. Cragg and P. T. C. So, Biophys. J. **78**, 248a (2000).
[5] B. Rothenhäusler and W. Knoll, Nature (London) **332**, 615 (1988).
[6] I. I. Smolyaninov, J. Elliott, A. V. Zayats, and C. Davis, Phys. Rev. Lett. **94**, 057401 (2005).
[7] N. Fang, H. Lee, C. Sun, and X. Zhang, Science **308**, 534 (2005).
[8] J.-J. Greffet and R. Carminati, Prog. Surf. Sci. **56**, 133 (1997).
[9] M. Dyba and S. Hell, Phys. Rev. Lett. **88**, 163901 (2002).
[10] M. Gustafsson, Proc. Natl. Acad. Sci. U.S.A. **102**, 13 081 (2005).
[11] R. Heintzmann, T. Jovin, and C. Cremer, J. Opt. Soc. Am. A **19**, 1599 (2002).
[12] V. Lauer, J. Microsc. **205**, 165 (2002).
[13] P. S. Carney and J. C. Schotland, J. Opt. Soc. Am. A **20**, 542 (2003).
[14] K. Belkebir, P. C. Chaumet, and A. Sentenac, J. Opt. Soc. Am. A **22**, 1889 (2005).
[15] D. Marks and P. S. Carney, Opt. Lett. **30**, 1870 (2005).
[16] E. N. Economou, Phys. Rev. **182**, 539 (1969).
[17] P. C. Chaumet and A. Sentenac, Phys. Rev. B **72**, 205437 (2005).
[18] M. Gustafsson, J. Microsc. **198**, 82 (2000).